Effects of nuclear deformation and neutron transfer in capture process, and origin of fusion hindrance at deep sub-barrier energies

V.V.Sargsyan[1,2], G.G.Adamian[1], N.V.Antonenko[1], W. Scheid[3], and H.Q.Zhang[4]

[1] *Joint Institute for Nuclear Research, 141980 Dubna, Russia*
[2] *International Center for Advanced Studies, Yerevan State University, M. Manougian 1, 0025, Yerevan, Armenia*
[3] *Institut für Theoretische Physik der Justus–Liebig–Universität, D–35392 Giessen, Germany*
[4] *China Institute of Atomic Energy, Post Office Box 275, Beijing 102413, China*
(Dated: December 1, 2011)

The roles of nuclear deformation and neutron transfer in sub-barrier capture process are studied within the quantum diffusion approach. The change of the deformations of colliding nuclei with neutron exchange can crucially influence the sub-barrier fusion. The comparison of the calculated capture cross section and the measured fusion cross section in various reactions at extreme sub-barrier energies gives us information about the fusion and quasifission.

I. INTRODUCTION

The nuclear deformation and neutron-transfer process have been identified as playing a major role in the magnitude of the sub-barrier capture and fusion cross sections [1]. There are a several experimental evidences which confirm the importance of nuclear deformation on the capture and fusion. The influence of nuclear deformation is straightforward. If the target nucleus is prolate in the ground state, the Coulomb field on its tips is lower than on its sides, that then increases the capture or fusion probability at energies below the barrier corresponding to the spherical nuclei. The role of neutron transfer reactions is less clear. A correlation between the overall transfer strength and fusion enhancement was firstly noticed in Ref. [2]. The importance of neutron transfer with positive Q-values on nuclear fusion (capture) originates from the fact that neutrons are insensitive to the Coulomb barrier and therefore they can start being transferred at larger separations before the projectile is captured by target-nucleus [3]. Therefore, it is generally thought that the sub-barrier fusion cross section will increase [4–8] because of the neutron transfer. As suggested in Ref. [9], the enhancements in fusion yields may be due to the transfer of a neutron pair with a positive Q-value. However, as shown recently in Ref. [10], the two-neutron transfer channel with large positive Q-value weakly influences the fusion (capture) cross section in the ^{60}Ni + ^{100}Mo reaction at sub-barrier energies. So, from the present data an unambiguous signature of the role of neutron transfer channel could not be inferred.

The experiments with various medium-light and heavy systems have shown that the experimental slopes of the complete fusion excitation function keep increasing at low sub-barrier energies and may become much larger than the predictions of standard coupled-channel calculations. This was identified as the fusion hindrance [11]. More experimental and theoretical studies of sub-barrier fusion hindrance are needed to improve our understanding of its physical reason, which may be especially important in astrophysical fusion reactions [12].

It is worth remembering that the first evidences of hindrance for compound nucleus formation in the reactions with massive nuclei ($Z_1 \times Z_2 > 1600$) at energies near the Coulomb barrier were observed at GSI already long time ago [13]. The theoretical investigations showed that the probability of complete fusion depends on the competition between the complete fusion and quasifission after the capture stage [14–16]. As known, this competition can strongly reduce the value of the fusion cross section and, respectively, the value of the evaporation residue cross section in the reactions producing superheavy nuclei. Although the quasifission was originally ascribed to the reactions with massive nuclei, it is the general phenomenon which is related to the binary decay of nuclear system after the capture, but before the compound nucleus formation which could exist at angular momenta treated. The mass and angular distributions of the quasifission products depend on the entrance channel and bombarding energy [14]. Because the capture cross section is the sum of the fusion and quasifission cross sections, from the comparison of calculated capture cross sections and measured fusion cross sections one can extract the hindrance factor and show a role of the quasifission channel in the reactions with various medium-mass and heavy nuclei at extreme sub-barrier energies.

In the present paper the quantum diffusion approach [17, 18] is applied to study the fusion hindrance and the roles of nuclear deformation and neutron transfer in sub-barrier capture process. With this approach many heavy-ion capture reactions at energies above and well below the Coulomb barrier have been successfully described [17–19]. Since the details of our theoretical treatment were already published in Refs. [17, 18], the model will be shortly described in Sec. II. The calculated results will be presented in Sec. III.

II. MODEL

In the quantum diffusion approach the collisions of nuclei are treated in terms of a single collective variable: the relative distance between the colliding nuclei. The nuclear deformation effects are taken into consider-

ation through the dependence of the nucleus-nucleus potential on the deformations and orientations of colliding nuclei. Our approach takes into consideration the fluctuation and dissipation effects in collisions of heavy ions which model the coupling with various channels. We have to mention that many quantum-mechanical and non-Markovian effects accompanying the passage through the potential barrier are taken into consideration in our formalism [17, 20, 21]. The details of used formalism are presented in our previous articles [17, 18]. All parameters of the model are set as in Ref. [17]. All calculated results are obtained with the same set of parameters and are rather insensitive to the reasonable variation of them [17, 18]. The heights of the calculated Coulomb barriers $V_b = V(R_b)$ (R_b is the position of the Coulomb barrier) are adjusted to the experimental data for the fusion or capture cross sections. To calculate the nucleus-nucleus interaction potential $V(R)$, we use the procedure presented in Refs. [17, 18]. For the nuclear part of the nucleus-nucleus potential, the double-folding formalism with the Skyrme-type density-dependent effective nucleon-nucleon interaction is used.

To analyze the experimental date on fusion cross section, it is useful to use the so called universal fusion function (UFF) F_0 [22]. The advantages of UFF appear clearly when one wants to compare fusion cross sections for systems with quite different Coulomb barrier heights and positions. In the reactions where the capture and fusion cross sections coincide, the comparison of experimental cross sections with the UFF allows us to make conclusions about the role of deformation of colliding nuclei and the nucleon transfer between interacting nuclei in the capture cross section because the UFF (the consequence of the Wong's formula) does not contain these effects. In Ref. [22] a reduction procedure was proposed to eliminate the influence of the nucleus-nucleus potential on the fusion cross section. It consists of the following transformations:

$$E_{\text{c.m.}} \to x = \frac{E_{\text{c.m.}} - V_b}{\hbar\omega}, \qquad \sigma^{exp} \to F(x) = \frac{2E_{\text{c.m.}}}{\hbar\omega R_b^2}\sigma^{exp}.$$

The frequency $\omega = \sqrt{V''(R_b)/\mu}$ is related with the second derivative $V''(R_b)$ of the total nucleus-nucleus potential $V(R)$ (the Coulomb + nuclear parts) at the barrier radius R_b and the reduced mass parameter μ. With these replacements one can compare the experimental data for different reactions. After these transformations, the reduced calculated fusion cross section takes the simple form

$$F_0 = \ln[1 + \exp(2\pi x)].$$

To take into consideration the deviation of the real potential from the inverted oscillator, we modify the reduction procedure as follows:

$$E_{\text{c.m.}} \to x = S/(\hbar\pi),$$

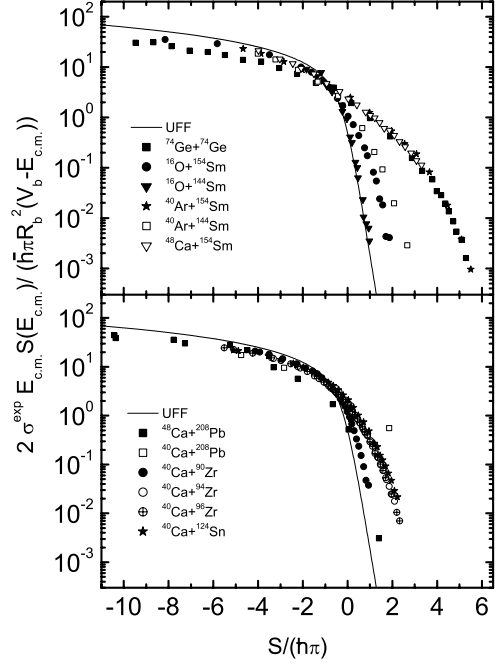$$\sigma^{exp} \to F(x) = \frac{2SE_{\text{c.m.}}}{\hbar\pi R_b^2(V_b - E_{\text{c.m.}})}\sigma^{exp}.$$

FIG. 1: Comparison of modified UFF F_0 with the experimental values of $\dfrac{2E_{\text{c.m.}}S(E_{\text{c.m.}})}{\hbar\pi R_b^2(V_b - E_{\text{c.m.}})}\sigma^{exp}$ for the indicated reactions. The experimental data for σ^{exp} are from Refs. [23–30].

In this case

$$F_0 = \ln[1 + \exp(-2S/\hbar)],$$

where $S(E_{\text{c.m.}})$ is the classical action. At energies above the Coulomb barrier, we have $S = \pi(V_b - E_{\text{c.m.}})/\omega$.

III. RESULTS OF CALCULATIONS

A. Effect of quadrupole deformation

In Fig. 1 (upper part), one can see the comparisons of dependencies F and F_0 on $S/(\hbar\pi)$ for some reactions considered in present paper. As expected, at sub-barrier energies the deviation from the UFF is larger in the case of reactions with strongly deformed target-nuclei and large factor $Z_1 \times Z_2$ (^{16}O,^{40}Ar,^{48}Ca+ ^{154}Sm, ^{74}Ge + ^{74}Ge). For the reactions ^{16}O,^{40}Ar+^{144}Sm with spherical targets the experimental cross sections are rather close to the UFF. To separate the effects of deformation and neutron transfer, firstly we consider the reactions with deformed nuclei in which Q-value for the neutron transfer are small, i.e. the neutron transfers can be disregarded. In Figs. 2 and 3, the calculated capture cross sections for the reactions ^{16}O,^{48}Ca,^{40}Ar+^{154}Sm, and ^{74}Ge+^{74}Ge are in a good agreement with the available experimental data [23, 24, 26, 27] showing that the quadrupole deformations of the interacting nuclei are the main reasons for the enhancement of the capture cross section at sub-
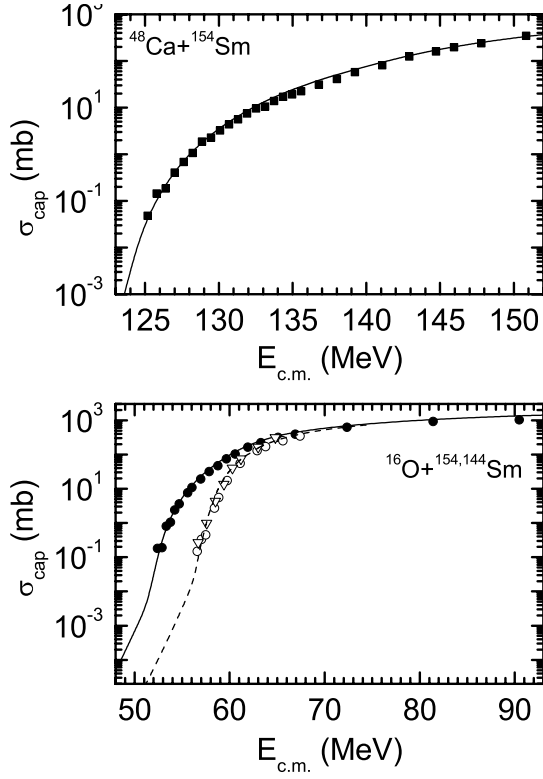
FIG. 2: The calculated capture cross sections versus $E_{\text{c.m.}}$ for the indicated reactions ^{16}O,^{48}Ca + ^{154}Sm (solid lines), and ^{16}O + ^{144}Sm (dashed line). The experimental data (symbols) are from Refs. [23–25]. The following quadrupole deformation parameters are used: $\beta_2(^{154}$Sm$)$=0.341 [31], $\beta_2(^{144}$Sm$)$=0.05, and $\beta_2(^{16}$O$)$=$\beta_2(^{48}$Ca$)$=0.

FIG. 3: The same as Fig. 2, for the indicated reactions ^{74}Ge+^{74}Ge, ^{40}Ar + ^{154}Sm (solid lines), and ^{40}Ar + ^{144}Sm (dashed line). The experimental data (symbols) are from Ref. [26, 27]. The following quadrupole deformation parameters are used: $\beta_2(^{40}$Ar$)$=0.25 [31], $\beta_2(^{74}$Ge$)$=0.2825 [31], $\beta_2(^{154}$Sm$)$=0.341 [31], and $\beta_2(^{144}$Sm$)$=0.05.

barrier energies. The quadrupole deformation parameters β_2 are taken from Ref. [31] for the deformed even-even nuclei. In Ref. [31] the quadropole deformation parameters β_2 for the first excited 2^+ states of nuclei are given. For the nuclei deformed in the ground state, the β_2 in 2^+ state is similar to the β_2 in the ground state and we use β_2 from Ref. [31] in the calculations. For double magic nuclei, in the ground state we take $\beta_2 = 0$. In Ref. [32] the experimentally observed enhancement of sub-barrier fusion for the reactions ^{16}O,^{48}Ca+^{154}Sm, and ^{74}Ge+^{74}Ge was explained by the nucleon transfer and neck formation effects. However, in the present article we demonstrate that a good agreement with the experimental data at sub-barrier energies could be reached taking only the quadrupole deformations of interacting nuclei into consideration. We should mention, that for the sub-barrier energies the results of calculations are very sensitive to the quadrupole deformation parameters β_2 of the interacting nuclei. Since there are uncertainties in the definition of the values of β_2 in the light- and the medium-mass nuclei, one can extract the quadrupole deformation parameters of these nuclei from the comparison of the calculated capture cross sections with the experimental data. The best case is when the projectile or target is
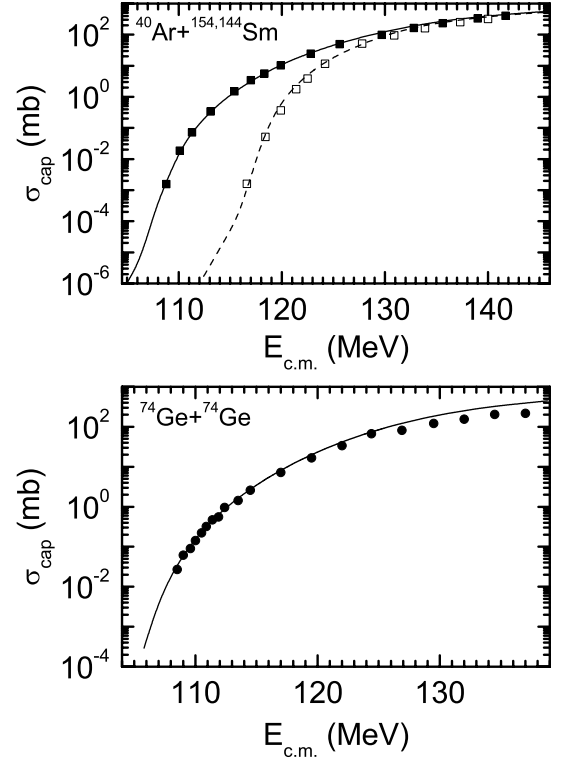
the spherical double magic nucleus and there are no neutron transfer channels with large positive Q-values. In this way by describing the reactions ^{28}Si + ^{90}Zr,^{144}Sm, ^{34}S + ^{168}Er, ^{36}S + ^{90,96}Zr, ^{40}Ar + ^{112,116,122}Sn,^{144}Sm, ^{58}Ni + ^{58}Ni, ^{64}Ni + ^{100}Mo,^{74}Ge (Figs. 5–10), we extract the following values of the quadrupole deformation parameter β_2=0.30, 0.125, 0, 0.25, 0.05, 0.087, 0, 0.08, 0.12, 0.11, 0.1, and 0.05 for the nuclei ^{28}Si, ^{34}S, ^{36}S, ^{40}Ar, ^{58}Ni, ^{64}Ni, ^{90}Zr, ^{96}Zr, ^{112}Sn, ^{116}Sn, ^{122}Sn, and ^{144}Sm, respectively. Note that almost the same values of quadrupole deformations parameters of nuclei in the ground state were predicted within the mean-field and the macroscopic-microscopic models [42]. For ^{40}Ar, ^{96}Zr, ^{112}Sn, ^{116}Sn, and ^{122}Sn the extracted β_2 for are equal to the experimental ones from Ref. [31]. These extracted deformation parameters we use in calculations in next subsection. Note t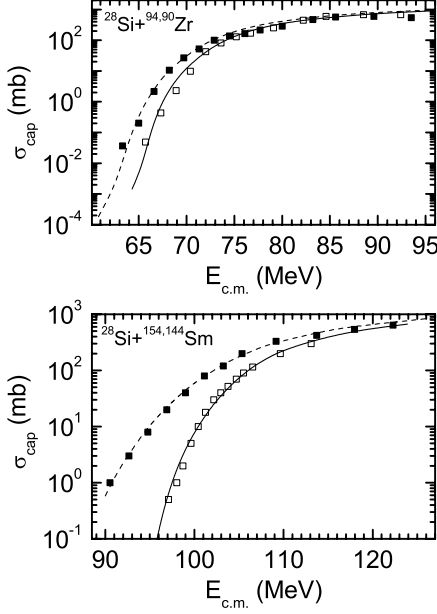hat almost the same values of quadrupole deformations parameters of nuclei in the ground state were predicted within the mean-field and the macroscopic-microscopic models [42]. For ^{40}Ar, ^{96}Zr, ^{112}Sn, ^{116}Sn, and ^{122}Sn the extracted β_2 for are equal to the experimental ones from Ref. [31]. These extracted deformation parameters we use in calculations in next subsection.

FIG. 4: The same as Fig. 2, for the indicated reactions ^{28}Si+^{94,90}Zr,^{154}Sm (solid lines), and ^{28}Si + ^{90}Zr,^{144}Sm (dashed lines). The experimental data (symbols) are from Refs. [33–35]. The following quadrupole deformation parameters are used: $\beta_2(^{154}$Sm$)$=0.341 [31], $\beta_2(^{144}$Sm$)$=0.05, and $\beta_2(^{28}$Si$)$=0.3.

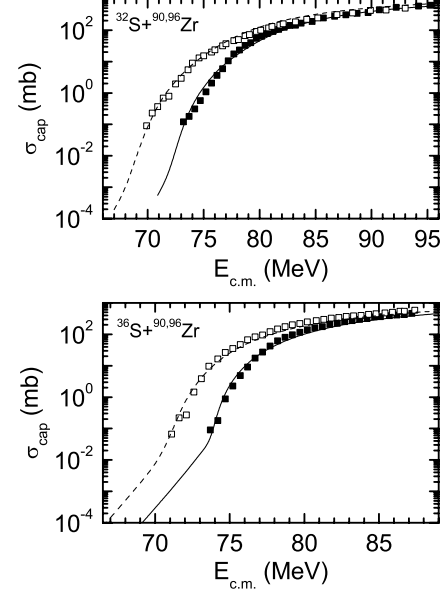FIG. 6: The same as Fig. 2, for the indicated reactions ^{36,32}S + ^{90}Zr (solid lines), and ^{36,32}S + ^{96}Zr (dashed lines). The experimental data (symbols) are from Refs. [36, 37]. The following quadrupole deformation parameters are used: $\beta_2(^{32}$S$)$=0.312 [31], $\beta_2(^{34}$S$)$=0.252 [31], $\beta_2(^{96}$Zr$)$=0.08, and $\beta_2(^{36}$S$)$=$\beta_2(^{90}$Zr$)$=0.

FIG. 5: The same as Fig. 2, for the indicated reactions ^{40}Ar + ^{112,122}Sn (solid lines), and ^{40}Ar + ^{116}Sn (dashed line). The experimental data (symbols) are from Ref. [27]. The following quadrupole deformation parameters are used: $\beta_2(^{112}$Sn$)$=0.1227 [31], $\beta_2(^{116}$Sn$)$=0.1118 [31], $\beta_2(^{122}$Sn$)$=0.1036 [31], and $\beta_2(^{40}$Ar$)$=0.25 [31].
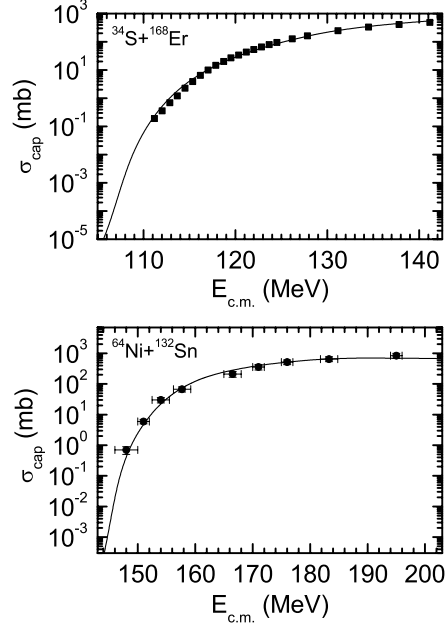

FIG. 7: The same as Fig. 2, for the indicated reactions ^{34}S + ^{168}Er and ^{64}Ni + ^{132}Sn. The experimental data (symbols) are from Refs. [38, 39]. The following quadrupole deformation parameters are used: $\beta_2(^{168}$Er$)$=0.3381 [31], $\beta_2(^{66}$Ni$)$=0.158 [31], $\beta_2(^{130}$Sn$)$=0, and $\beta_2(^{34}$S$)$=0.125.
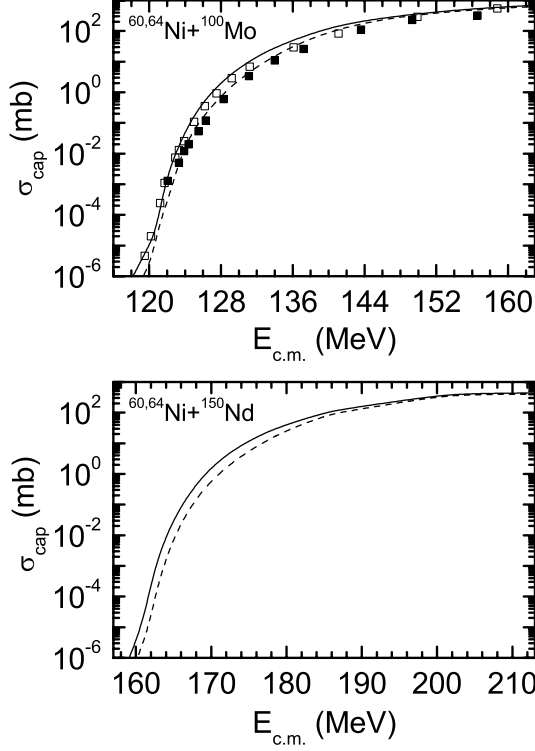
FIG. 8: The same as Fig. 2, for the indicated reactions ^{64}Ni + ^{100}Mo,^{150}Nd (solid lines) and ^{60}Ni + ^{100}Mo,^{150}Nd (dashed lines). The experimental data (symbols) for the ^{64}Ni + ^{100}Mo reaction are from Ref. [40]. The following quadrupole deformation parameters are used: $\beta_2(^{62}$Ni$)$=0.1978 [31], $\beta_2(^{98}$Mo$)$=0.1684 [31], $\beta_2(^{100}$Mo$)$=0.2309 [31], $\beta_2(^{148}$Nd$)$=0.2036 [31], $\beta_2(^{150}$Nd$)$=0.2848 [31], and $\beta_2(^{64}$Ni$)$=0.087.

FIG. 9: The same as Fig. 2, for the indicated reactions ^{40}Ca + ^{96}Zr,^{208}Pb (dashed lines), ^{40}Ca + ^{90}Zr (solid line), and ^{48}Ca + ^{208}Pb (solid line and open squares and triangles). For the reactions ^{40}Ca + ^{96}Zr,^{208}Pb, the calculated capture cross sections without taking into consideration the neutron transfer process are shown by dotted lines. The experimental data (symbols) are from Refs. [28–30]. The following quadrupole deformation parameters are used: $\beta_2(^{42}$Ca$)$=0.247 [31], $\beta_2(^{94}$Zr$)$=0.09 [31], $\beta_2(^{96}$Zr$)$=0.08, and $\beta_2(^{40}$Ca$)$=$\beta_2(^{48}$Ca$)$=$\beta_2(^{90}$Zr$)$=$\beta_2(^{206,208}$Pb$)$=0.

B. Effect of neutron transfer

Several experiments were performed to understand the effect of neutron transfer in the fusion (capture) reactions. The choice of the projectile-target combination is crucial, and for the systems studied one can make unambiguous statements regarding the neutron transfer process with a positive Q-value when the interacting nuclei are double magic or semi-magic spherical nuclei. In this case one can disregard the strong nuclear deformation effects. The good examples are the reactions with the spherical nuclei: ^{40}Ca + ^{208}Pb (Q_{2n}=5.7 MeV) and ^{40}Ca + ^{96}Zr (Q_{2n}=5.5 MeV). In Fig. 1 (lower part), one can see that the reduced capture cross sections in these reactions strongly deviate from the UFF in contrast to those in the reactions ^{48}Ca + ^{208}Pb and ^{48}Ca + ^{96}Zr, where the neutron transfer channels are suppressed (the negative Q-values). Since the transfer of protons is shielded by the Coulomb barrier, it occurs when two nuclei almost touch
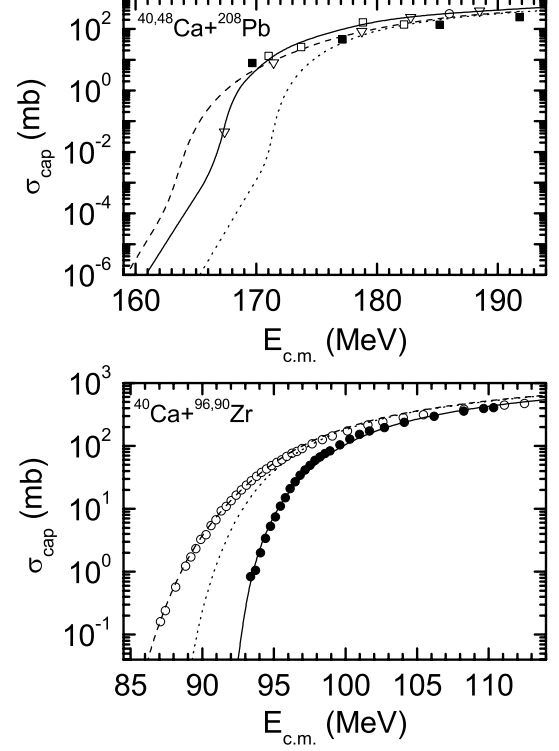
each other [43], i.e. after a capture. Thus, the proton transfer can be disregarded in the calculations of capture cross sections. Following the hypothesis of Ref. [9], we assume that the sub-barrier capture mainly depends on the two-neutron transfer with the positive and relatively large Q-value. Our assumption is that, before the projectile is captured by target-nucleus (before the crossing of the Coulomb barrier) which is the slow process, the two-neutron transfer occurs at larger separations that can lead to the population of the first 2^+ state in the recipient nucleus [44]. Since after two-neutron transfer the mass numbers, the deformation parameters of interacting nuclei, and, respectively, the height and shape of the Coulomb barrier are changed, one can expect the enhancement or suppression of the capture. For example, after the neutron transfer in the reaction ^{40}Ca$(\beta_2 = 0)$ + ^{208}Pb$(\beta_2 = 0) \rightarrow {}^{42}Ca(\beta_2 = 0.247)$ + ^{206}Pb$(\beta_2 = 0)$
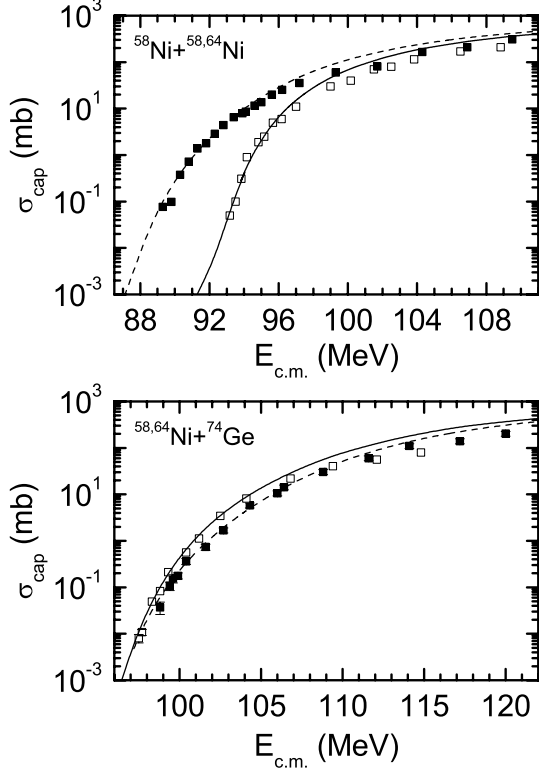
FIG. 10: The same as Fig. 2, for the indicated reactions ^{58}Ni + ^{64}Ni,^{74}Ge (dashed lines) and ^{58}Ni + ^{58}Ni, ^{64}Ni + ^{74}Ge (solid lines). The experimental data (symbols) are from Ref. [41]. The following quadrupole deformation parameters are used: $\beta_2(^{60}$Ni)=0.207 [31], $\beta_2(^{72}$Ge)=0.2424 [31], $\beta_2(^{74}$Ge)=0.2825 [31], $\beta_2(^{58}$Ni)=0.05, and $\beta_2(^{62}$Ni)$\approx \beta_2(^{64}$Ni)=0.087.

(^{40}Ca($\beta_2 = 0$) + ^{96}Zr($\beta_2 = 0.08$)$\rightarrow^{42}$Ca($\beta_2 = 0.247$) + ^{94}Zr($\beta_2 = 0.09$)) the deformation of the nuclei increases and the mass asymmetry of the system decreases and thus the value of the Coulomb barrier decreases and the capture cross section becomes larger (Fig. 10). We observe the same behavior in the reactions ^{64}Ni + ^{132}Sn (Fig. 7), ^{58}Ni+^{64}Ni,^{74}Ge (Fig. 9), ^{32}S+^{96}Zr, ^{40}Ca+^{94}Zr (Fig. 11), ^{40}Ca+^{192}Os,^{198}Pt (Fig. 12), and ^{40}Ca + ^{48}Ca,^{116,124}Sn (Fig. 13). One can see a good agreement between the calculated results and the experimental data. For some reactions at energies above the Coulomb barrier, the small deviation between the calculated results and experimental data probably arises from the fact that the fusion-fission channel was not taken into consideration in the experimental capture cross sections. So, our results show that the observed capture enhancement at sub-barrier energies for the reactions mentioned above is related to the two-neutron transfer channel. For these reactions there is a large deflection from the UFF (see lower part of Fig. 1). Note that strong population of
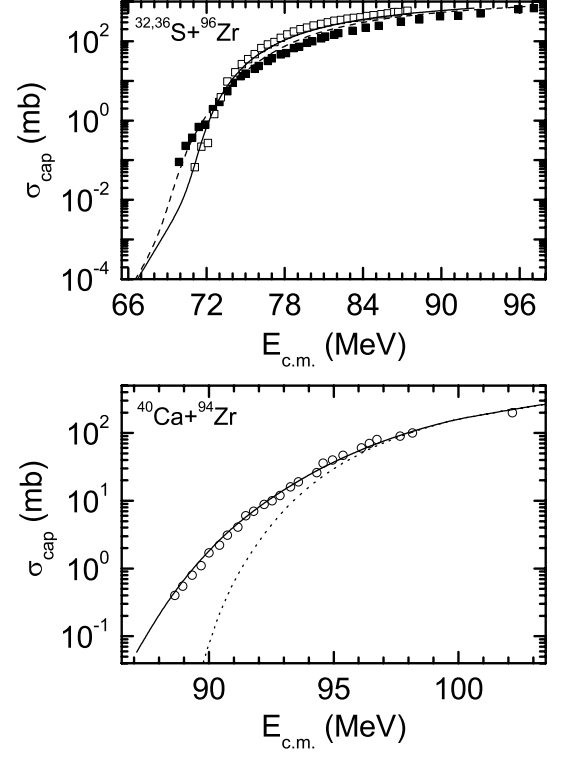
FIG. 11: The same as Fig. 2, for the indicated reactions ^{40}Ca + ^{94}Zr (solid line), ^{32}S + ^{96}Zr (dashed line and solid squares), and ^{36}S + ^{96}Zr (solid line and open squares). For the ^{40}Ca + ^{94}Zr reaction, the calculated capture cross sections without taking into consideration the neutron transfer process are shown by dotted line. The experimental data (symbols) are from Refs. [36, 37, 45]. The following quadrupole deformation parameters are used: $\beta_2(^{42}$Ca)=0.247 [31], $\beta_2(^{94}$Zr)=0.09 [31], $\beta_2(^{92}$Zr)=0.1028 [31], $\beta_2(^{96}$Zr)=0.08, and $\beta_2(^{36}$S)=$\beta_2(^{40}$Ca)=0.

the yrast states, and in particular of the first 2^+ state of even Ar (Ca) isotopes via the neutron pick-up channels in the ^{40}Ar + ^{208}Pb (^{40}Ca + ^{96}Zr) reaction is experimentally found in Ref. [44]. In the calculations, for such excited recipient nuclei we use the experimental deformation parameters β_2 related to the first 2^+ states from the table of Ref. [31]. We assume that after two neutron transfer the residues of donor nuclei remain in the ground state with corresponding quadrupole deformation.

One can find the reactions with large positive two-neutron transfer Q-values where the transfer weakly influences or even suppresses the capture process. This happens if after transfer the deformations of nuclei almost do not change or even decrease. For instance, in the reactions ^{32}S($\beta_2 = 0.312$) + ^{96}Zr($\beta_2 = 0.08$)$\rightarrow^{34}$S($\beta_2 = 0.252$) + ^{94}Zr($\beta_2 = 0.09$), ^{60}Ni($0.05 < \beta_2 \lesssim 0.1$) + ^{100}Mo($\beta_2 = 0.231$)$\rightarrow^{62}$Ni($\beta_2 = 0.198$) + ^{98}Mo($\beta_2 = $
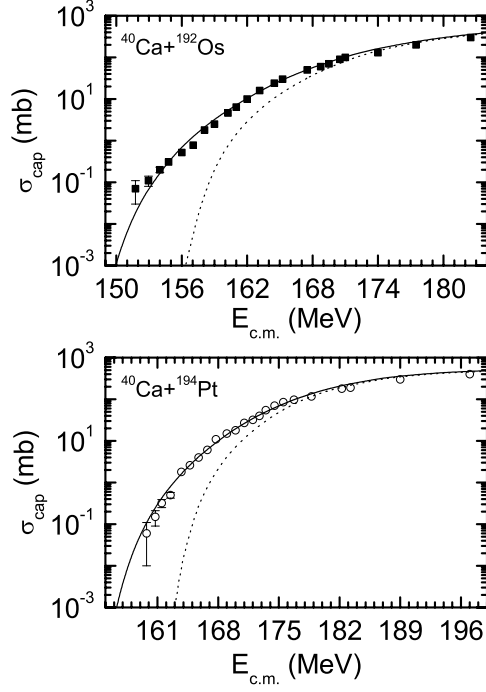
FIG. 12: The same as Fig. 2, for the indicated reactions ^{40}Ca + ^{192}Os,^{194}Pt (solid lines). The calculated capture cross sections without taking into consideration the neutron transfer process are shown by dotted lines. The experimental data (symbols) are from Ref. [46]. The following quadrupole deformation parameters are used: $\beta_2(^{42}$Ca$)=0.247$ [31], $\beta_2(^{192}$Os$)=0.1667$ [31], $\beta_2(^{190}$Os$)=0.1775$ [31], $\beta_2(^{194}$Pt$)=0.1426$ [31], $\beta_2(^{192}$Pt$)=0.1532$ [31], and $\beta_2(^{40}$Ca$)=0$.

FIG. 13: The same as Fig. 2, for the indicated reactions ^{40}Ca + ^{48}Ca,^{116}Sn (solid lines), and ^{40}Ca + ^{124}Sn (dashed line). The experimental data (symbols) are from Refs. [47–49]. The following quadrupole deformation parameters are used: $\beta_2(^{42}$Ca$)=0.247$ [31], $\beta_2(^{116}$Sn$)=0.1118$ [31], $\beta_2(^{122}$Sn$)=0.1036$ [31], and $\beta_2(^{46}$Ca$)=\beta_2(^{40}$Ca$)=0$.

0.168) and ^{60}Ni$(0.05 < \beta_2 \lesssim 0.1)$ + ^{150}Nd$(\beta_2 = 0.285)\rightarrow^{62}Ni(\beta_2 = 0.198)$ + ^{148}Nd$(\beta_2 = 0.204)$ one can expect weak dependence of the capture cross section on the neutron transfer (Figs. 8 and 11). There is the experimental indication of such effect for the ^{60}Ni + ^{100}Mo reaction [10]. The weak influence of neutron transfer on the capture process is also found in the reactions ^{32}S + ^{110}Pd ,^{154}Sm,^{208}Pb (Figs. 14 and 15), ^{28}Si + ^{94}Zr,^{142}Ce,^{154}Sm,^{208}Pb (Figs. 4 and 16). The same behaviour is expected in the reactions ^{84}Kr + ^{138}Ce,^{140}Nd. For these reactions, the effect of quadrupole deformations of interacting nuclei is much stronger than the effect of neutron transfer between the interacting nuclei.

Note that our model predicts almost the same capture cross sections for the reactions with positive Q-values ^{6}He,^{9}Li,^{11}Be + ^{206}Pb, ^{18}O + ^{58}Ni and for the reactions without neutron transfer ^{4}He,^{7}Li,^{9}Be + ^{208}Pb, ^{16}O + ^{60}Ni, respectively.

In Fig. 17, the capture cross sections for the reactions ^{58,64}Ni + ^{207}Pb are predicted. As seen, there is considerable difference between the capture cross sections in these two reactions because of the existence of the two-neutron transfer channel $(Q_{2n}=5.6$ MeV) in the reaction
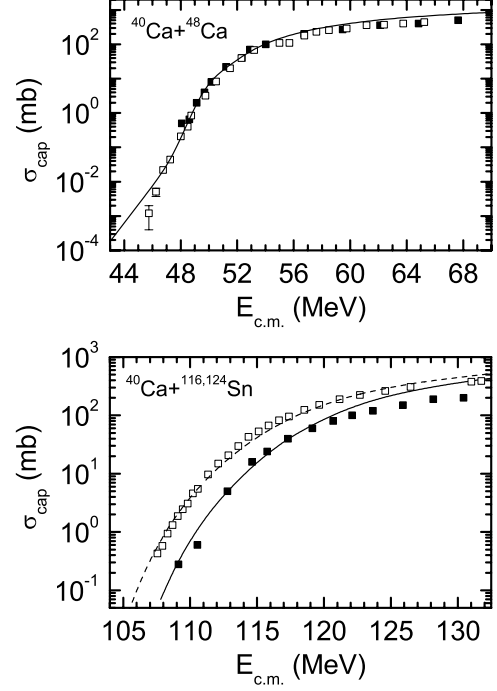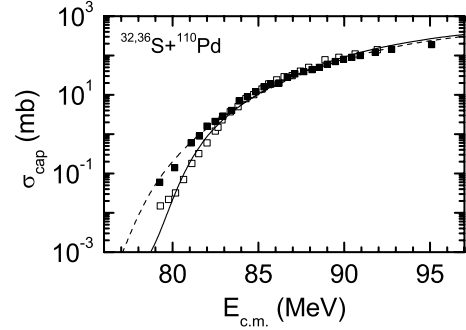

FIG. 14: The same as Fig. 2, for the indicated reactions ^{32}S + ^{110}Pd (dashed line and closed squares) and ^{36}S + ^{110}Pd (solid line and open squares). The experimental data (symbols) are from Ref. [6]. The following quadrupole deformation parameters are used: $\beta_2(^{34}$S$)=0.252$ [31], $\beta_2(^{108}$Pd$)=0.243$ [31], $\beta_2(^{110}$Pd$)=0.257$ [31], and $\beta_2(^{36}$S$)=0$.
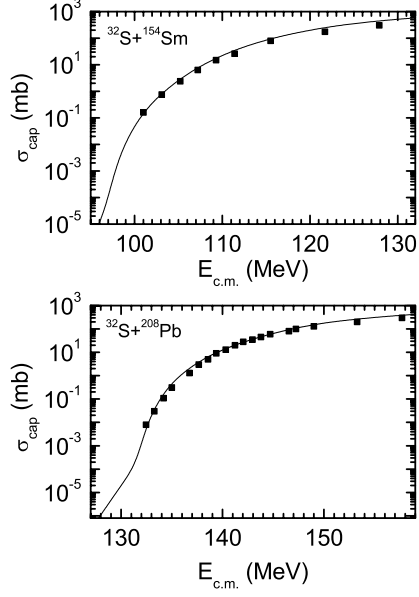
FIG. 15: The same as Fig. 2, for the indicated reactions ^{32}S + ^{154}Sm,^{208}Pb. The experimental data (symbols) are from Refs. [6]. The following quadrupole deformation parameters are used: $\beta_2(^{34}$S$)$=0.252 [31], $\beta_2(^{152}$Sm$)$=0.3064 [31], and $\beta_2(^{206}$Pb$)$=0.
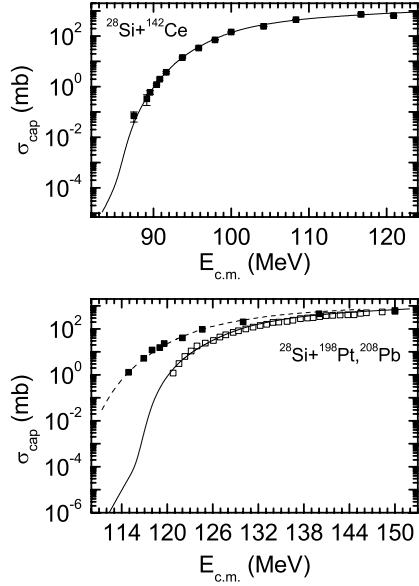

FIG. 16: The same as Fig. 2, for the indicated reactions ^{28}Si + ^{142}Ce,^{208}Pb (solid lines), and ^{28}Si + ^{198}Pt (dashed line). The experimental data (symbols) are from Refs. [52–54]. The following quadrupole deformation parameters are used: $\beta_2(^{30}$Si$)$=0.315 [31], $\beta_2(^{140}$Ce$)$=0.1012 [31], $\beta_2(^{196}$Pt$)$=0.1296 [31], and $\beta_2(^{206}$Pb$)$=0.
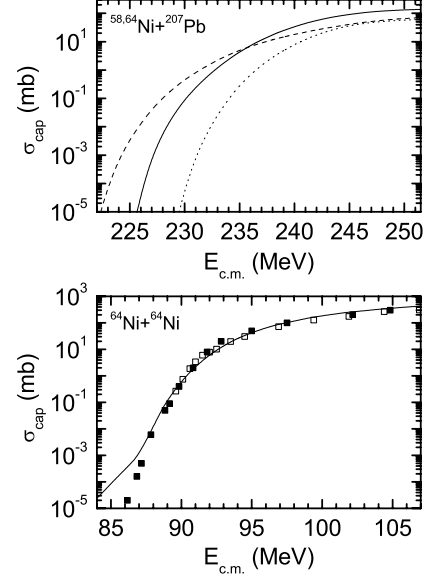

FIG. 17: The same as Fig. 2, for the indicated reactions ^{58}Ni + ^{207}Pb (dashed line), ^{64}Ni + ^{64}Ni (solid line), and ^{64}Ni + ^{207}Pb (solid line). For the ^{58}Ni + ^{207}Pb reaction, the calculated capture cross sections without taking into consideration the neutron transfer process are shown by dotted line. The experimental data (symbols) are from Refs. [41, 56]. The following quadrupole deformation parameters are used: $\beta_2(^{60}$Ni$)$=0.207 [31], $\beta_2(^{58}$Ni$)$=0.05, $\beta_2(^{64}$Ni$)$=0.087, and $\beta_2(^{205,207}$Pb$)$=0.

^{58}Ni + ^{207}Pb$\rightarrow^{60}$Ni + ^{205}Pb. Thus, the study of these reactions could be a good test for the conclusion about the effect of neutron transfer. It will be interesting to compare the role of the neutron transfer channel in the reactions with spherical nuclei mentioned above (Fig. 10) and with deformed targets, ^{40}Ca + ^{154}Sm,^{238}U (Fig. 18).

Due to a change of the regime of interaction (the turning-off of the nuclear forces and friction) at sub-barrier energies [17–19], the curve related to the capture cross section as a function of bombarding energy has smaller slope (see Figs. 2–8,10,11,13–16). This effect is more visible in the capture of spherical nuclei without the neutron transfer. However, the present experimental data at strongly sub-barrier energies are rather poor.

IV. ORIGIN OF FUSION HINDRANCE IN REACTIONS WITH MEDIUM-MASS NUCLEI AT DEEP SUB-BARRIER ENERGIES

Since the sum of the fusion cross section σ_{fus} and the quasifission cross section σ_{qf} gives the capture cross section
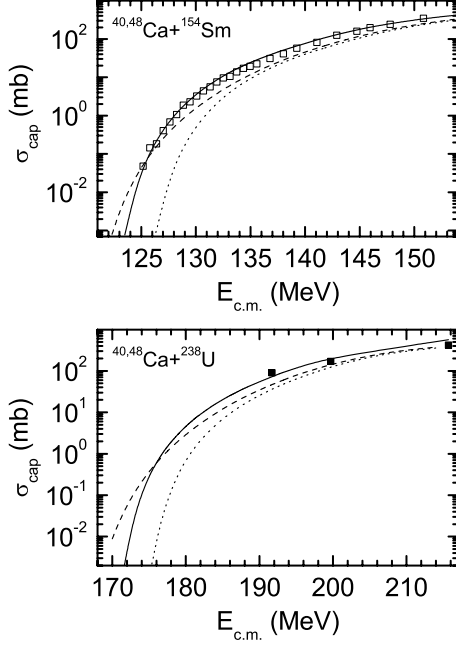
$$\sigma_{cap} = \sigma_{fus} + \sigma_{qf},$$

FIG. 18: The same as Fig. 2, for the indicated reactions ^{40}Ca + ^{154}Sm,^{238}U (dashed lines), and ^{48}Ca + ^{154}Sm,^{238}U (solid lines). For the reactions ^{40}Ca + ^{154}Sm,^{238}U, the calculated capture cross sections without taking into consideration the neutron transfer process are shown by dotted line. The experimental data (symbols) for the reactions ^{48}Ca + ^{154}Sm,^{238}U are from Refs. [23, 55]. The following quadrupole deformation parameters are used: $\beta_2(^{42}$Ca$)=0.247$ [31], $\beta_2(^{152}$Sm$)=0.3055$ [31], $\beta_2(^{154}$Sm$)=0.341$ [31], $\beta_2(^{236}$U$)=0.2821$ [31], $\beta_2(^{238}$U$)=0.2863$ [31], and $\beta_2(^{48}$Ca$)=0$.

FIG. 19: The same as Fig. 2, for the indicated reactions ^{36}S + ^{48}Ca,^{64}Ni. The experimental data (symbols) are from Refs. [57, 58]. The following quadrupole deformation parameters are used: $\beta_2(^{64}$Ni$)=0.087$ and $\beta_2(^{36}$S$)=\beta_2(^{48}$Ca$)=0$.

one can estimate the relative contributions of σ_{fus} and σ_{qf} to σ_{cap}. In Figs. 17, 13 and 19 the calculated capture cross section are presented for the reactions ^{40}Ca + ^{48}Ca, ^{64}Ni + ^{64}Ni and ^{36}S + ^{48}Ca,^{64}Ni. As seen, at energies above and just below the Coulomb barriers $\sigma_{cap} = \sigma_{fus}$. The difference between the sub-barrier capture and fusion cross sections becomes larger with decreasing bombarding energy $E_{c.m.}$. The same effect one can see for the ^{16}O + ^{208}Pb reaction [17]. Assuming that the estimated capture and the measured fusion cross sections are correct, the small fusion cross section at energies well below the Coulomb barrier may indicate that other reaction channel is preferable and the system goes to this channel after the capture. The observed hindrance factor may be understood in term of quasifission whose cross section should be added to the σ_{fus} to obtain a meaningful comparison with the calculated capture cross section. At deep sub-barrier energies, the quasifission event corresponds to the formation of a nuclear-molecular state or dinuclear system with small excitation energy that separates (in the competition with the compound nucleus formation process) by the quantum tunneling through the Coulomb barrier in a
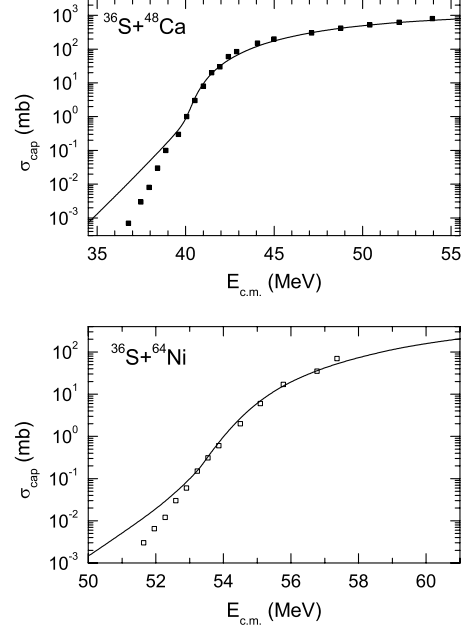
binary event with mass and charge close to the entrance channel. In this sense the quasifission is the general phenomenon which takes place in the reactions with the massive [13–16], medium-mass and, probably, light nuclei. For the medium-mass and light nuclei, this reaction channel is expected to be at deep sub-barrier energies and has to be studied in the future experiments: from the measurement of the mass (charge) distribution in the collisions with total momentum transfer one can show the distinct components due to the quasifission. Because these energies the angular momentum $J < 10$, the angular distribution would have small anisotropy. The low-energy experimental data would probably provide straight information since the high-energy data may be shaded by competing nucleon transfer processes. Note that the binary decay events were already observed experimentally in Ref. [59] for the ^{58}Ni + ^{124}Sn reaction at energies below the Coulomb barrier but assumed to be related to deep-inelastic scattering. At energies above the Coulomb barrier the hindrance to fusion was revealed in Ref. [60] for the reactions ^{58}Ni + ^{124}Sn and ^{16}O + ^{208}Pb.

V. SUMMARY

The quantum diffusion approach was applied to study the capture process in the reactions with deformed and spherical nuclei at sub-barrier energies. The avail-

able experimental data at energies above and below the Coulomb barrier are well described. As shown, the experimentally observed sub-barrier fusion enhancement is mainly related to the quadrupole deformation of the colliding nuclei and neutron transfer with large positive Q-value. The change of the magnitude of the capture cross section after the neutron transfer occurs due to the change of the deformations of nuclei. When after the neutron transfer the deformations of nuclei do not change or slightly decrease, the neutron transfer weakly influences or even suppresses the capture process. It would be interesting to study such-type of reactions.

The importance of quasifission near the entrance channel was noticed for the reactions with medium-mass nuclei at extreme sub-barrier energies. The quasifission can explain the difference between the capture and fusion cross sections. One can try to check experimentally these predictions.

[1] A.B. Balantekin and N. Takigawa, Rev. Mod. Phys. **70**, (1998) 77; L.F. Canto, P.R.S. Gomes, R. Donangelo, and M.S. Hussein, Phys. Rep. **424**, (2006) 1.

[2] W. Henning, F.L.H. Wolfs, J.P. Schiffer, and K.E. Rehm, Phys. Rev. Lett. **58**, 318 (1987).

[3] P.H. Stelson, H.J. Kim, M. Beckerman, D. Shapira, and R.L. Robinson, Phys. Rev. C **41**, 1584 (1990). C.L. Jiang, K.E. Rehm, J. Gehring, B. Glagola, W. Kutschera, M. Rhein, and A.H. Wuosmaa, Phys. Lett. B **337**, 59 (1994).

[4] R. Pengo *et al.*, Nucl. Phys. **A411**, 255 (1983).

[5] R.B. Roberts *et al.*, Phys. Rev. C **47**, R1831 (1993).

[6] A.M. Stefanini, D. Ackermann, L. Corradi, J.H. He, G. Montagnoli, S. Beghini, F. Scarlassara, and G.F. Segato, Phys. Rev. C **52**, R1727 (1995).

[7] D. Ackermann *et al.*, Nucl. Phys. **A609**, 91 (1996).

[8] A.A. Sonzogni, J.D. Bierman, M.P. Kelly, J.P. Lestone, J.F. Liang, and R. Vandenbosch, Phys. Rev. C **57**, 722 (1998).

[9] R. Broglia, C.H. Dasso, S. Landowne, and A. Winther, Phys. Rev. C **27**, 2433 (1983); R. Broglia, C.H. Dasso, S. Landowne, and G. Pollarolo, Phys. Lett. B **133**, 34 (1983).

[10] F. Scarlassara *et al.*, EPJ Web of Conf. **17**, 05002 (2011) .

[11] C.L. Jiang *et al.*, Phys. Rev. Lett. **89**, 052701 (2002).

[12] K. Langanke and C.A. Barnes, Adv.Nucl.Phys. **22**, (1996) 173. A. Aprahamian, K. Langanke, and M. Wiescher, Prog.Part.Nucl.Phys. **54**, (2005) 535.

[13] J.G. Keller *et al.*, Nucl. Phys. **A452**, 173 (1986).

[14] V.V. Volkov, Particles and Nuclei, **35**, 797 (2004).

[15] G.G. Adamian, N.V. Antonenko, and W.Scheid, Phys. Rev. C **68**, 034601 (2003); *Lecture Notes in Physics, Clusters in Nuclei*, Vol. 2, ed. by C. Beck (Springer, Berlin, 2011) in print.

[16] G. Giardina *et al.*, Nucl. Phys. **A671**, 165 (2000); A. Nasirov *et al.*, Nucl. Phys. **A759**, 342 (2005); Z.-Q. Feng, G.-M. Jin, J.-Q. Li, and W. Scheid, Phys. Rev. C **76**, 044606 (2007); H.Q. Zhang *et al.*, Phys. Rev. C **81**, 034611 (2010).

[17] V.V. Sargsyan, G.G. Adamian, N.V. Antonenko, and W. Scheid, Eur. Phys. J. A **45**, 125 (2010).

[18] V.V. Sargsyan, G.G. Adamian, N.V. Antonenko, W. Scheid, and H.Q. Zhang, Eur. Phys. J. A **47**, 38 (2011).

[19] V.V. Sargsyan, G.G. Adamian, N.V. Antonenko, W. Scheid, and H.Q. Zhang, J. of Phys.: Conf. Ser. **282**, 012001 (2011); EPJ Web of Conf. **17**, 04003 (2011).

[20] V.V. Sargsyan, Z. Kanokov, G.G. Adamian, N.V. Antonenko, and W. Scheid, Phys. Rev. C **80**, 034606 (2009); Phys. Rev. C **80**, 047603 (2009).

[21] G.G. Adamian, N.V. Antonenko, Z. Kanokov, and V.V. Sargsyan, Teor. Mat. Fiz. **145**, 87 (2005) [Theor. Math. Phys. **145**, 1443 (2006)]; Z. Kanokov, Yu.V. Palchikov, G.G. Adamian, N.V. Antonenko, and W. Scheid, Phys. Rev. E **71**, 016121 (2005); Yu.V. Palchikov, Z. Kanokov, G.G. Adamian, N.V. Antonenko, and W. Scheid, Phys. Rev. E **71**, 016122 (2005).

[22] L.F. Canto, P.R.S. Gomes, J. Lubian, L.C. Chamon, and E. Crema, J. Phys. G **36**, 015109 (2009); Nucl. Phys. **A821**, 51 (2009).

[23] G.N. Knyazheva *et al.*, Phys. Rev. C **75**, 064602 (2007); A.M. Stefanini *et al.*, Eur. Phys. J. A **23**, 473 (2005).

[24] J.R. Leigh *et al.*, Phys. Rev. C **52**, 3151 (1995).

[25] D.E. DiGregorio *et al.*, Phys. Rev. C **39**, 516 (1989).

[26] M. Beckerman *et al.*, Phys. Rev. C **28**, 1963 (1983).

[27] W. Reisdorf *et al.*, Nucl. Phys. **A438**, 212 (1985).

[28] H. Timmers *et al.*, Nucl. Phys. **A633**, 421 (1998).

[29] A.J. Pacheco *et al.*, Phys. Rev. C **45**, 2861 (1992); R. Bock *et al.*, Nucl. Phys. **A388**, 334 (1982).

[30] E. Prokhorova *et al.*, Nucl. Phys. **A802**, 45 (2008).

[31] S. Raman, C.W. Nestor, Jr, and P. Tikkanen, At. Data Nucl. Data Tables **78**, 1 (2001).

[32] J.M.B. Shorto *et al.*, Phys. Rev. C **81**, 044601 (2010).

[33] S. Kalkal *et al.*, Phys. Rev. C **81**, 044610 (2010).

[34] S. Gil *et al.*, Phys. Rev. Lett. **65**, 3100 (1990).

[35] G.P.A. Nobre *et al.*, Phys. Rev. C **75**, 044606 (2007).

[36] H.Q. Zhang *et al.*, Phys. Rev. C **82**, 054609 (2010).

[37] A.M. Stefanini *et al.*, Phys. Rev. C **62**, 014601 (2000).

[38] C.R. Morton *et al.*, Phys. Rev. C **62**, 024607 (1999).

[39] J.F. Liang *et al.*, Phys. Rev. C **78**, 047601 (2008).

[40] C.L. Jiang *et al.*, Phys. Rev. C **71**, 044613 (2005).

[41] M. Beckerman *et al.*, Phys. Rev. C **25**, 837 (1982).

[42] P. Möller *et al.*, At. Data Nucl. Data Tables **59**, 185 (1995).

[43] G.G. Adamian, A.K. Nasirov, N.V. Antonenko, and R.V. Jolos, Phys. Part. Nucl. **25**, 583 (1994).

[44] S. Szilner *et al.*, Phys. Rev. C **76**, 024604 (2007); L. Corradi, G. Pollarolo, and S. Szilner, J. Phys. G **36**, 113101 (2009); S. Szilner *et al.*, J. of Phys.: Conf. Ser. **282**, 012021 (2011); EPJ Web of Conf. **17**, 03005 (2011); Phys. Rev. C **84**, 014325 (2011); L. Corradi *et al.*, EPJ Web of Conf. **17**, 08004 (2011); Phys. Rev. C **84**, 034603 (2011).

[45] A.M. Stefanini *et al.*, Phys. Rev. C **76**, 014610 (2007).

[46] J.D. Bierman *et al.*, Phys. Rev. C **54**, 3068 (1996).

[47] H.A. Aljuwair *et al.*, Phys. Rev. C **30**, 1223 (1984).

[48] C.L. Jiang *et al.*, Phys. Rev. C **82**, 041601R (2010).

[49] A.M. Stefanini *et al.*, Eur. Phys. J. A **23**, 1401 (1997); F. Scarlassara *et al.*, Nucl. Phys. **A672**, 99 (2000).

[50] P.R.S. Gomes *et al.*, Phys. Rev. C **49**, 245 (1994).

[51] M. Dasgupta and D.J. Hinde, Nucl. Phys. **A734**, 148 (2004).

[52] S. Gil *et al.*, Phys. Rev. C **51**, 1336 (1995).

[53] K. Nishio, H. Ikezoe, S. Mitsuoka, and J. Lu, Phys. Rev. C **62**, 014602 (2000).

[54] D.J. Hinde *et al.*, Nucl. Phys. **A592**, 271 (1995).

[55] W.Q. Shen *et al.*, Phys. Rev. C **36**, 115 (1987).

[56] C.L. Jiang *et al.*, Phys. Rev. Lett. **93**, 012701 (2004).

[57] A.M. Stefanini *et al.*, Phys. Rev. C **78**, 044607 (2008).

[58] G. Montagnoli *et al.*, Nucl. Phys. **A834**, 159c (2010); Phys. Rev. C **82**, 064609 (2010).

[59] F.L.H. Wolfs, W. Henning, K.E. Rehm, and J.P. Schiffer, Phys. Lett. B **196**, 113 (1987).

[60] G. Pollarolo, Nucl. Phys. **A787**, 206c (2007).